ORIGINAL RESEARCH

Three Unique Interstitial Macrophages in the Murine Lung at Steady State

Sophie L. Gibbings[1], Stacey M. Thomas[1], Shaikh M. Atif[1], Alexandra L. McCubbrey[2], A. Nicole Desch[3], Thomas Danhorn[4], Sonia M. Leach[4], Donna L. Bratton[3], Peter M. Henson[1,3], William J. Janssen[2,5], and Claudia V. Jakubzick[1,3]

[1]Department of Pediatrics, National Jewish Health, Denver, Colorado; [2]Department of Medicine, National Jewish Health, Denver, Colorado; [3]Integrated Department of Immunology, National Jewish Health and University of Colorado Denver Anschutz Campus, Denver, Colorado; [4]Integrated Center for Genes, Environment and Health, National Jewish Health, Denver, Colorado; and [5]Division of Pulmonary Sciences and Critical Care, University of Colorado Denver, Denver, Colorado

Abstract

The current paradigm in macrophage biology is that some tissues mainly contain macrophages from embryonic origin, such as microglia in the brain, whereas other tissues contain postnatal-derived macrophages, such as the gut. However, in the lung and in other organs, such as the skin, there are both embryonic and postnatal-derived macrophages. In this study, we demonstrate in the steady-state lung that the mononuclear phagocyte system is comprised of three newly identified interstitial macrophages (IMs), alveolar macrophages, dendritic cells, and few extravascular monocytes. We focused on similarities and differences between the three IM subtypes, specifically, their phenotype, location, transcriptional signature, phagocytic capacity, turnover, and lack of survival dependency on fractalkine receptor, CX_3CR1. Pulmonary IMs were located in the bronchial interstitium but not the alveolar interstitium. At the transcriptional level, all three IMs displayed a macrophage signature and phenotype. All IMs expressed MER proto-oncogene, tyrosine kinase, CD64, CD11b, and CX_3CR1, and were further distinguished by differences in cell surface protein expression of CD206, Lyve-1, CD11c, CCR2, and MHC class II, along with the absence of Ly6C, Ly6G, and Siglec F. Most intriguingly, in addition to the lung, similar phenotypic populations of IMs were observed in other nonlymphoid organs, perhaps highlighting conserved functions throughout the body. These findings promote future research to track four distinct pulmonary macrophages and decipher the division of labor that exists between them.

Keywords: monocytes; dendritic cells; pulmonary; interstitial macrophages; mononuclear phagocytes

Clinical Relevance

The presence of macrophages in the lung interstitium has long been accepted, but how to distinguish them from other mononuclear phagocytes and where they are located is unclear. Here, we describe three unique interstitial macrophages (IMs) that coexist with alveolar macrophages, two dendritic cells, and constitutively trafficking $Ly6C^+$ monocytes. We performed a comprehensive analysis, for the first time, of three unique IM populations present in the murine lung. Transcriptome analysis suggests that there are functional differences between the three IMs. IMs are located in the bronchial interstitium and not in the alveolar interstitium. Most interestingly, similar IMs were observed in other organs, perhaps highlighting their conserved function throughout the body.

(Received in original form November 8, 2016; accepted in final form February 21, 2017)

This work was supported by National Institutes of Health grants R01HL115334 (C.V.J.), R01HL109517 (W.J.J.), R01HL34303 and R01AI110408 (D.L.B), and R01HL68864 and R01HL88138 (P.M.H.).

Author Contributions: S.L.G., P.M.H., W.J.J., and C.V.J. prepared the manuscript; S.L.G., S.M.T., S.M.A., A.L.M. and A.N.D. executed experiments; T.D., S.M.L. and D.L.B. executed the transcriptome analysis; all authors provided intellectual input, critical feedback, discussed results, and designed experiments.

Correspondence and requests for reprints should be addressed to Claudia V. Jakubzick, Ph.D., National Jewish Health, Department of Pediatrics, 1400 Jackson Street, Denver, CO 80206. E-mail: jakubzickc@njhealth.org

This article has an online supplement, which is accessible from this issue's table of contents at www.atsjournals.org

Am J Respir Cell Mol Biol Vol 57, Iss 1, pp 66–76, Jul 2017

Originally Published in Press as DOI: 10.1165/rcmb.2016-0361OC on March 3, 2017
Internet address: www.atsjournals.org

The naive, nonstimulated lung contains a number of different types of resident mononuclear phagocytes. These include monocytes, dendritic cells (DCs), and macrophages. Resident alveolar macrophages (AMs) present in the alveolar air space have been extensively studied, are now known to arise during embryogenesis, and are ontologically distinct from cells derived from postnatal hematologic origin (1–3). Earlier studies of the so-called "marginating" pool of pulmonary leukocytes emphasized that a substantial proportion of circulating monocytes at any point in time reside within the pulmonary microvasculature. In addition, it has been shown in the naive animal that the lung contains another population of macrophages, distinct from AMs, monocytes, and DCs (4, 5): the interstitial macrophages (IMs). These IMs have not been well characterized, in part because of difficulties in identification and isolation. Moreover, their precise location within the lung has been controversial.

The innate immune system is increasingly recognized as a crucial contributor to tissue homeostasis, both for the recognition and removal of external or endogenous insults as well as for the maintenance of normal tissue structure and function. This is especially relevant in the lung, due to its continuous and extensive exposure to the environment. The lack of defined information about the nature and location of the pulmonary IMs provided the stimulus for this study, in which we characterized their phenotype and turnover at baseline in the "normal" lung to thereby set the stage for understanding their roles in health and disease. Here, new techniques for identification, isolation, and characterization of IMs in normal, young-adult, C57BL/6 mice were employed, and have resulted in the description of three separable and substantially self-renewing populations of macrophages. These IMs exhibited different transcriptomal profiles, and were shown to be located in the interstitium of the bronchovascular bundles, but not in the alveolar walls. Notably, preliminary comparison with other tissues also showed three similar populations of IMs to be present in heart, gut, and skin.

Materials and Methods

Mice

Cluster of differentiation (CD) 45.1 and CD45.2 C57BL/6 mice were purchased from Jackson Laboratory (Bar Harbor, ME) and Charles River Laboratories (Worcester, MA). $CCR2^{-/-}$, $CX_3CR1^{GFP/GFP}$, $Zbtb46^{GFP/GFP}$, $IFN\gamma^{YFP}$, IL-12 $p40^{YFP}$, IL-10^{GFP} (Tiger), and MaFIA ($Csfr1^{GFP}$) mice were purchased from Jackson Laboratory and bred in house. IL-4^{GFP} (4Get) mice were acquired from Dr. Philippa Marrack (Denver, CO). Mice were used at 6–10 weeks of age, housed in a specific pathogen-free environment at National Jewish Health (Denver, CO), and used in accordance with protocols approved by the Institutional Animal Care and Use Committee.

Bone Marrow Chimeras

Protection of lung macrophages during irradiation was performed as previously described (6). CD45.1 recipient wild-type mice were anesthetized with Avertin using 300 μl per mouse with tert-amyl alcohol content at 2.5% and 2,2,2 tribromoethanol (T1420; TCI America, Portland, OR) at a concentration of 50 mg/kg, and positioned between lead strips 1-cm thick by 2-cm wide to protect the lungs from radiation. γ radiation (900 Gy) from a cesium-131 source was used. CD45.2 bone marrow (BM) cells were prepared by flushing donor femurs and tibias with PBS. Cells were counted and transferred into recipient mice after radiation exposure. Chimeric mice were used for studies at 5 weeks after radiation and BM transfer.

Parabiosis

Parabiotic mice were created using a previously published protocol (7). Briefly, mice were continuously anesthetized with isofluorane and kept on a heated pad throughout surgery. Animal partners were shaved on opposing sides followed by an incision from the elbow to the knee. First, joints of the elbows and knees were sutured together using 3–0 nonabsorbable sutures. Then, dorsal–dorsal and ventral–ventral skin was joined using an absorbable 5–0 Vicryl suture. Finally, mice were administered carprofen for pain relief, as needed, and were kept on antibiotic Septra diet to prevent postoperative infections.

Preparation of Single-Cell Suspensions from Organs

Blood was drawn by cardiac puncture using a 26-gauge syringe coated with 100 mM EDTA to prevent coagulation, followed by lysis with BD Pharm lyse (BD Biosciences, San Jose, CA) red blood cell lysis buffer. Bronchoalveolar lavage was obtained by flushing the airways four times with 1 ml of cold PBS only. Mice were perfused via the heart with 20 ml of PBS. Lung and heart tissues were finely minced with scissors before digestion. The dorsal and ventral sides of the ears were separated before floating dermis-side down on digestion solution. Lungs and ear skin were digested with 500 μg/ml Liberase (Roche/Sigma, Branford, CT/St. Louis, MO). The heart was digested using collagenase D (Roche/Sigma) at 2.5 mg/ml for 30 minutes at 37°C. Single-cell suspensions were obtained by repeated glass pipetting before cells were filtered through a 100-μm nylon filter. Colon samples were prepared by first flushing and incubating gut tissue with buffer containing EDTA to deplete gut epithelial cells. The remaining colon tissue was minced and digested with a mixture of 0.85 mg/ml collagenase VIII and 1.2 mg/ml collagenase D (Roche, Branford, CT) to obtain single-cell suspensions. In some instances, cells of interest were enriched by MACS bead purification (Miltenyi, San Diego, CA) using either anti-CD11c and anti-CD11b microbeads, or biotinylated anti-MerTK using anti-biotin microbeads before analysis.

To differentiate intravascular and extravascular leukocytes, mice were injected intravenously with PE- or APC-conjugated anti-CD45 antibody 3 minutes before organ harvest.

Flow Cytometry

Single-cell suspensions were resuspended in FACS buffer containing HBSS with 0.3 μM EDTA and 0.2% FBS, and stained for 30 minutes with biotinylated anti-MerTK, followed by conjugated antibodies and conjugated streptavidin for a further 30 minutes. Table E1 in the online supplement outlines the complete list of antibodies used. For the analysis of BrdU incorporation, BrdU was administered by intraperitoneal injection of 1 mg per mouse daily for the time points indicated. Intracellular BrdU was detected according to the protocol from eBioscience (Waltham, MA). FACS data were acquired using the LSR II or LSR Fortessa (both BD Biosciences), and data were analyzed with FlowJo software (Ashland, Oregon). 4′,6-diamidino-2-phenylindole was added immediately before acquisition to exclude dead cells.

Microscopy

Frozen sections from $CX_3CR1^{GFP/+}$ reporter mice were prepared by inflating the lungs with a mixture of 20% sucrose: 1% paraformaldehyde: 50% optimum cutting temperature reagent, after perfusion with 1% paraformaldehyde. Sections (10 μm) were stained with anti-MerTK– or eF660-conjugated lymphatic vessel endothelial hyaluronan receptor 1 (Lyve-1) overnight, followed by Cy3-conjugated anti-goat antibody. Sections were imaged using Marianis (Denver, CO) or Zeiss (Denver, CO) fluorescent microscopes and analyzed with Slidebook (Denver, CO) and Image J (Bethesda, MD) software.

Phagocytosis Assays

For the *in vivo* assay, mice were anesthetized with Avertin, as described subsequently here, and intranasally instilled with a 50-μl suspension of *Escherichia coli* bioparticles (10^8 particles per mouse; Life Technologies, Carlsbad, CA), zymosan bioparticles (4×10^6 particles per mouse; Life Technologies), or carboxylated latex beads (10^9 per mouse; Polysciences, Warrington, PA). After 3 hours, lungs were harvested for flow cytometric assessment of particle uptake. For the *ex vivo* assay, whole-lung digests were enriched for viable hematopoietic cells by Percoll gradient centrifugation. *E. coli* or zymosan bioparticles or carboxylated latex beads were fed to enriched macrophages *ex vivo* and uptake was assessed by flow cytometry after 1-hour incubation at 37°C. Trypan blue was added to quench extracellular fluorescent particles 2 minutes before FACS analysis.

Macrophage RNA-seq Analysis

Extract protocol. Mice were killed and lungs perfused with PBS, finely minced, and digested by incubation in 0.5 mg/ml Liberase enzyme mix for 30 minutes. IMs and AMs were enriched using biotinylated anti-MerTK and anti-biotin MACS beads (Miltenyi). Enriched lung cells were then FACS sorted using the FACS Aria Fusion (BD Biosciences; strategy shown in Figure E2 in the online supplement). RNA was extracted from approximately 50,000 cells using the RNeasy Microkit (Qiagen, Hilden, Germany), as described in the manufacturer's protocols.

Library construction protocol. SMART-Seq v4 Ultra Low Input RNA Kit for Sequencing (Clontech, Mountview, CA), followed by Covaris (Woburn, MA) shearing and finished with Kapa Hyper prep kit (Wilmington, MA) using modified Life Technologies indexes.

Library strategy. All total RNA was run on a Bioanalyzer pico chip (Aligent, Santa Clara, CA) before library build with RIN scores from 9.2 to 10.0. All samples were started with 2 ng of total RNA (based on the

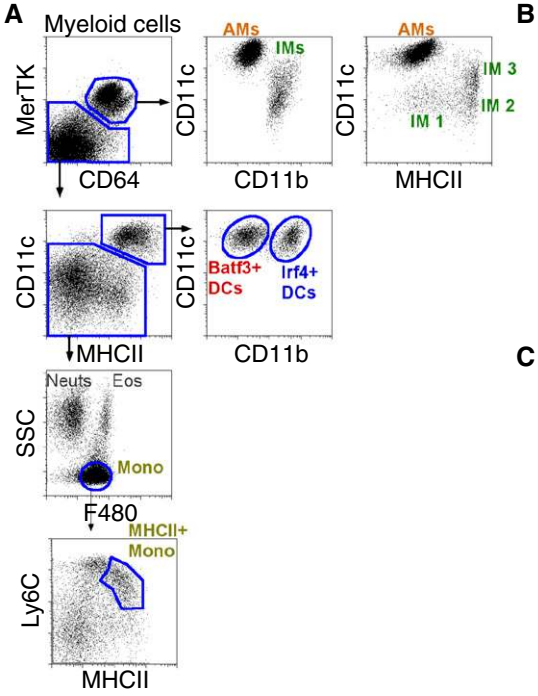

B

Pulmonary Cell Type	% Extravascular Myeloid Cells (±SEM)	Total # per lung (x10^5 ±SEM)
Alveolar Macrophages	75.8 ±3.75	32.22 ±0.17
Interstitial Macrophages	9.3 ±1.48	3.95 ±0.07
Ly6C$^+$ MHCII$^+$ Monocytes	0.82 ±0.24	0.35 ±0.01
Batf3$^+$ Dendritic Cells	6.42 ±0.25	2.73 ±0.01
Irf4$^+$ Dendritic Cells	4.58 ±0.25	1.94 ±0.01

C

Interstitial Macrophage	% Total IMs (±SEM)
IM1	26.38 ±1.45
IM2	27.63 ±1.53
IM3	44.50 ±1.93

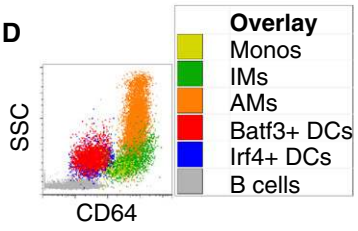

Figure 1. Analysis of pulmonary mononuclear phagocytes. (*A*) FACS gating strategy used to identify pulmonary interstitial macrophages (IMs) among other myeloid cells in naive mice. Myeloid cells were gated on CD11c versus CD11b (Figure E1A). Total myeloid cells were then plotted as MerTK versus CD64. *Top row*, the MerTK$^+$CD64$^+$ macrophage gate was plotted as CD11c versus CD11b or MHCII to illustrate the alveolar macrophages (AMs) and three IMs. *Top middle row*, MerTK$^-$CD64$^-$ macrophage–deficient gate was plotted with CD11c and MHCII to illustrate the dendritic cells (DCs). CD11c$^+$MHCII$^+$ DCs were plotted as CD11c versus CD11b to identify CD11b^{lo} (Batf3$^+$) and CD11b^{hi} (Irf4$^+$) DCs. *Bottom middle row*, macrophage/DC–deficient gate was plotted as side scatter (SSC) versus F4/80 to identify neutrophils (Neuts), eosinophils (Eos), and monocytes (Mono). *Bottom row*, monocytes were plotted as Ly6C versus MHCII to illustrate MHCII$^+$ monocytes. (*B*) Frequency of individual myeloid subtypes as a proportion of the total lung extravascular myeloid cells and total number per lung. (*C*) Frequency of IM subtypes as a proportion of the total IM pool. Data represent four independent experiments ($n = 4$). (*D*) Pulmonary mononuclear phagocytes were plotted as SSC versus CD64 to illustrate the granularity of pulmonary mononuclear phagocytes. MHC, major histocompatibility complex.

pico chip). After library build, samples were run on a High Sensitivity DNA qubit assay (measuring 2 ul of library), diluted to roughly 1 ng/ul and run on a High Sensitivity DNA bioanalyzer chip (Santa Clara, CA). All samples were pooled together and run on Ion Proton P1 chips.

Reads of at least 30 nt length were mapped to the mm10 release of the mouse genome using STAR (version 2.5.1b; https://doi.org/10.1093/bioinformatics/bts635) with splice site information from the Ensembl version 78 gene annotation (http://dec2014.archive.ensembl.org/). Read numbers and alignment quality metrics can be found in Figure E7.

Reads mapping uniquely to each gene of the Ensembl 78 annotation were quantified with the featureCounts program from the subread software package (version 1.5.0p-1) (8).

To identify genes with significant expression changes between macrophage types, an analysis of deviance was performed on the raw counts using the package, DESeq2 (version 1.8.1) (9) in R (version 3.2.0) (10) by comparing a model with the cell type and the replicate (pool of mice from which cells were extracted) as variables to a reduced model considering only the replicate using the likelihood ratio test. The replicate is incorporated to correct for any differences in individual mouse pools. For pairwise comparisons between macrophage types, we used a statistical model considering cell types and replicates from the entire data set and extracted contrasts between macrophage type pairs from the results of the Wald test.

Kyoto Encyclopedia of Genes and Genomes (KEGG) pathway analysis. Lists of up- and down-regulated genes with an adjusted *P* value of less than 0.1 from pairwise comparisons were tested separately for enrichment in KEGG pathways using the hypergeometric test in R 3.2.0 (11).

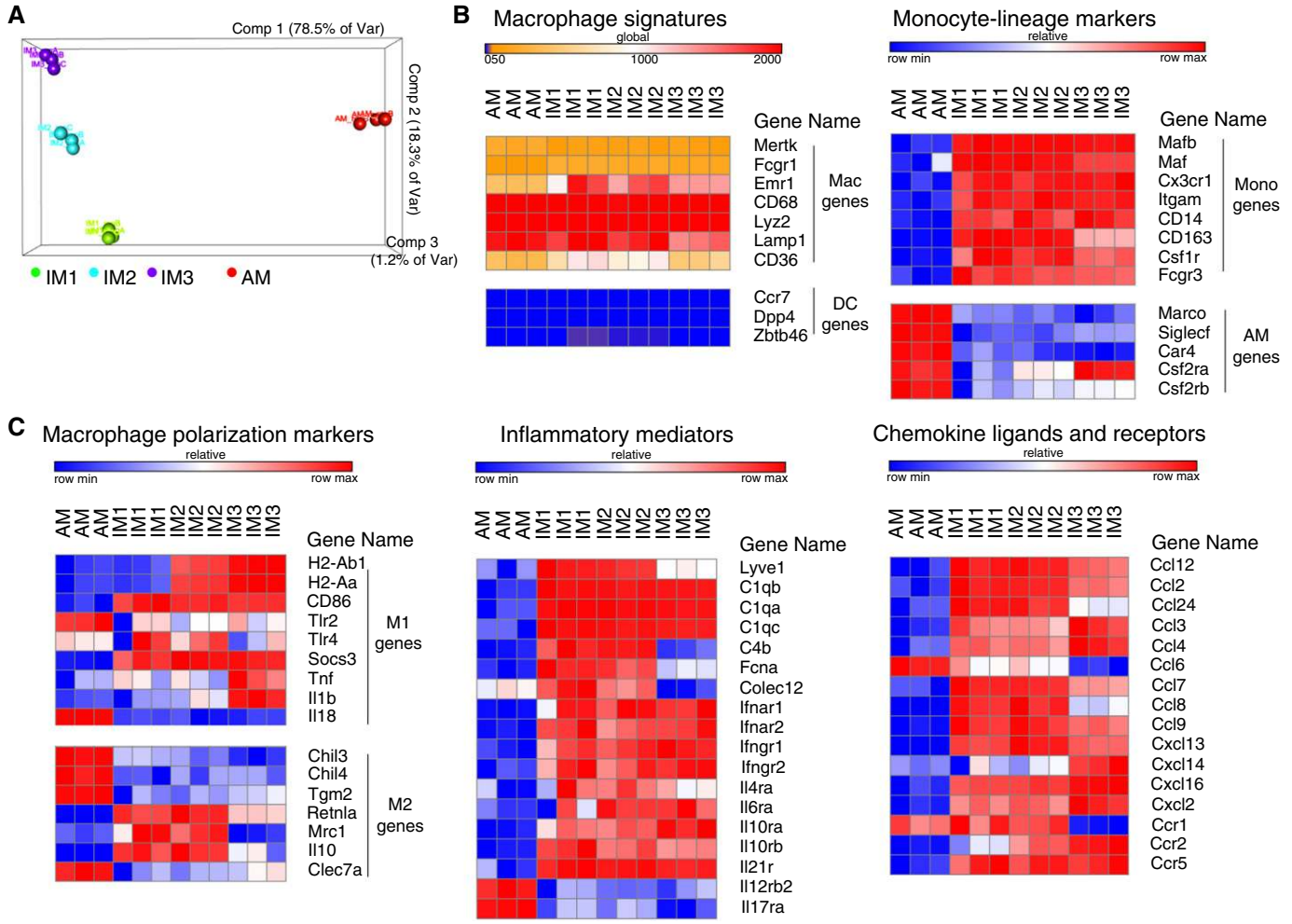

Figure 2. IMs are transcriptionally distinct from other pulmonary mononuclear phagocytes. Defined pulmonary myeloid cells, AMs, IM1, IM2, and IM3, from naive mice were sorted in triplicates for RNA sequencing analysis. (*A*) Principal component analysis plot illustrates IMs clustering distal from AMs and separate from each other. (*B* and *C*) Heat maps demonstrate RNA transcript expression from AM, IM1, IM2, and IM3. Genes of interest were separated into (*B*) macrophage- and monocyte-lineage–associated genes and (*C*) functional molecules: M1/M2 polarization markers; inflammatory mediators; chemokine ligands; and receptors. *Rows* are displayed as signal intensity relative to minimum and maximum values, with the exception of macrophage signature genes, where expression intensity is scaled globally across all genes of interest. *P* values and transcript per million (TPM) values are shown in Tables E2 and E3. Comp, component. Mac, macrophage.

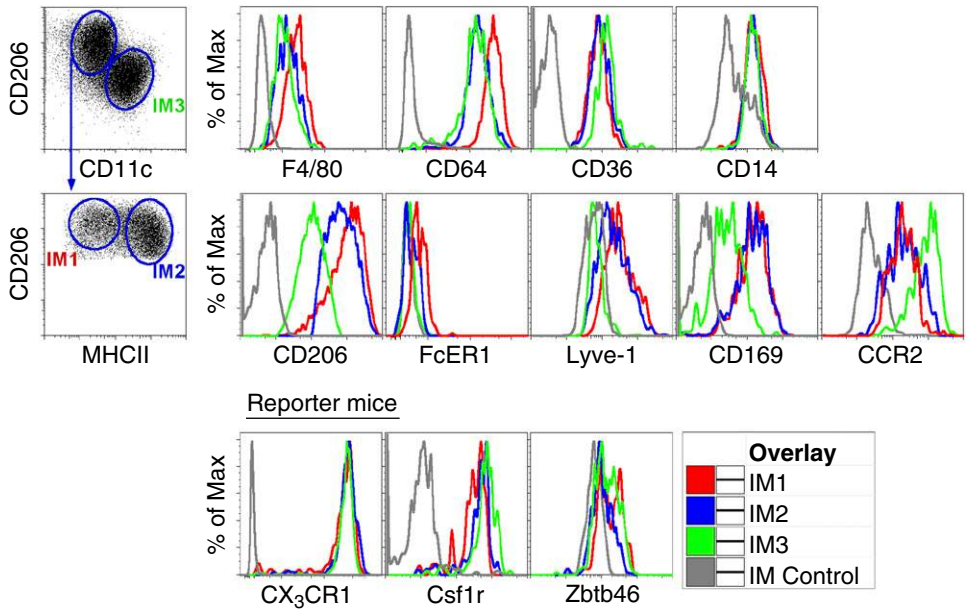

Figure 3. IMs display distinct cell surface protein expression. *Left*, FACS plot demonstrates how to identify IM1, IM2, and IM3 from $CD45^+MerTK^+CD64^+CD11b^+$ IMs. First, plotting CD206 versus CD11c separates IM3 from IM1 and IM2. $CD206^{int/hi}CD11c^{lo}$ cells were then plotted by MHCII to identify IM1 and IM2. *Top* and *middle rows,* histograms display overlays of all three IMs (IM1, *red*; IM2, *blue*; and IM3, *green*) for the given protein, relative to isotype antibody control (*gray*). *Bottom row*, reporter mice display histograms for the expression of CX_3CR1, Csfr1, and Zbtb46 in all three IMs relative to a control mouse (*gray*).

Heat maps were generated using the GENE-E software (http://www.broadinstitute.org/cancer/software/GENE-E/index.html) from the Broad Institute (Boston, MA). RNA-seq data were submitted to Gene Expression Omnibus (GEO): accession no. GSE94135.

Statistical Analysis

Statistical analysis was conducted using Prism software (GraphPad Software, Inc., San Diego, CA). All bar graphs are expressed

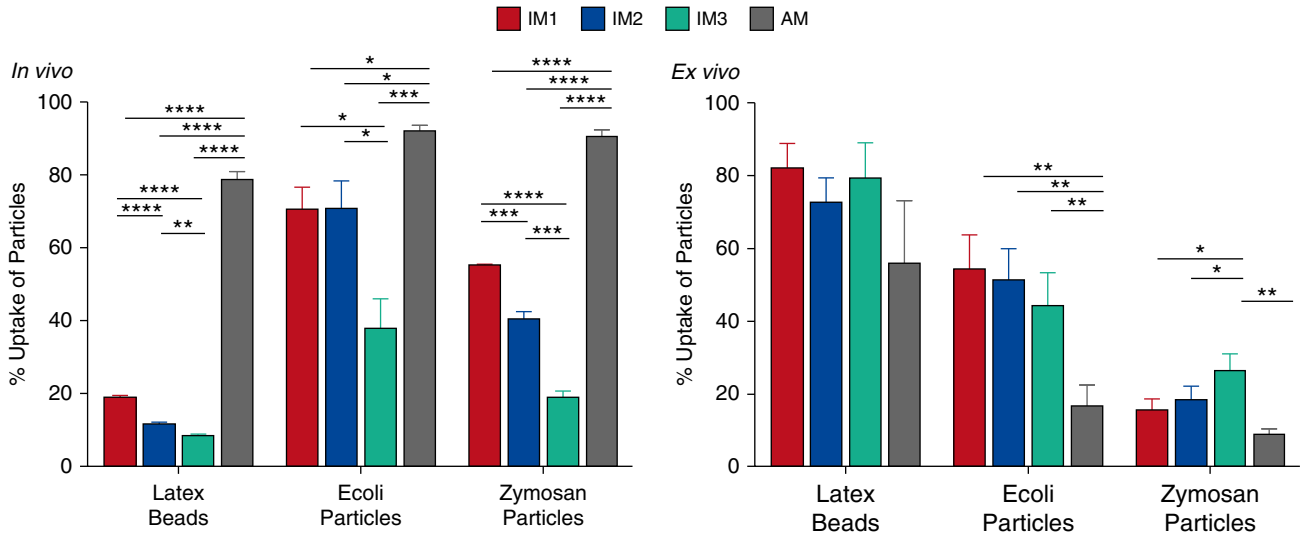

Figure 4. Phagocytic capacity of IMs *in vivo* and *ex vivo. In vivo*, carboxylated latex beads, *Escherichia coli*, or zymosan bioparticles were delivered via the intranasal route. Particle uptake was assessed after 3 hours. Data are representative of two experiments with $n = 3$ per group. *Ex vivo*, Percoll-enriched pulmonary macrophages were given carboxylated beads or bioparticles in culture. Particle uptake was assessed after 1 hour. Data are representative of three experiments with $n = 3$ per group. $^{****}P < 0.0005$, $^{***}P < 0.001$, $^{**}P < 0.005$, $^{*}P < 0.05$.

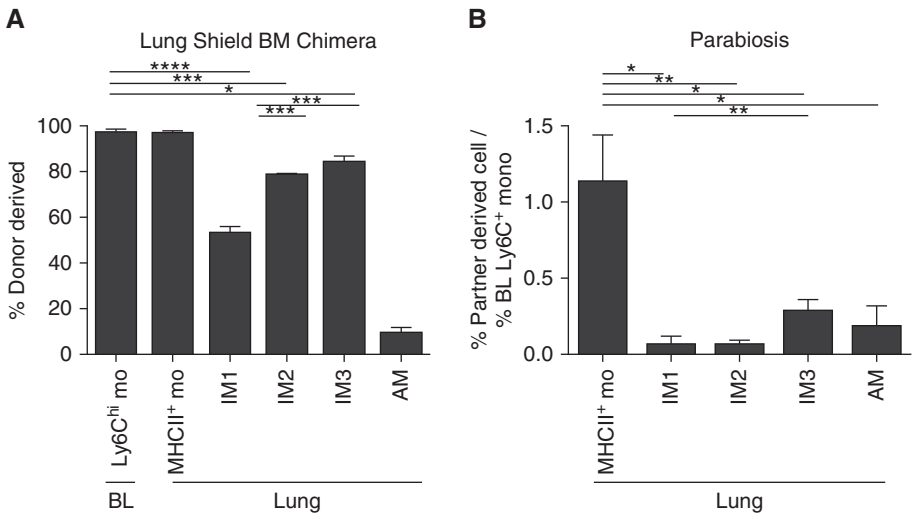

Figure 5. IMs are slowly replaced by circulating bone marrow (BM)-derived cells. (*A*) Wild-type mice were irradiated using lead strips to protect the lungs before delivery of congenic donor BM cells. Lung mononuclear phagocytes were analyzed for donor origin 5 weeks after BM reconstitution. Data are representative of two experiments with $n = 4$. BL, blood. (*B*) Parabiotic mice: 15 weeks after surgical joining of congenic wild-type (WT) mice (CD45.1 and CD45.2), the contribution of circulating partner-derived cells to the lung mononuclear phagocytes was analyzed. Data are represented as the ratio of partner-derived lung mononuclear phagocytes to partner-derived blood Ly6C$^+$ monocytes within the same mouse. Data are representative of two experiments with $n = 4$. $^{****}P < 0.0005$, $^{***}P < 0.001$, $^{**}P < 0.005$, $^{*}P < 0.05$. mo, monocytes.

as the mean (±SEM). Statistical tests were performed using two-tailed Student's *t* test and ANOVA. A *P* value less than 0.05 was considered statistically significant.

Results

Identification and Transcriptome Analyses of Pulmonary IMs in the Naive Mouse

As a first step toward comprehensively identifying all pulmonary macrophages, flow cytometry analysis was performed on single cells isolated from naive mouse lungs. Previous work has demonstrated that the coexpression of MerTK and CD64 specifically identifies all macrophages within numerous organs, including the lung (12). Therefore, to identify pulmonary macrophages, we first plotted all myeloid cells as MerTK versus CD64 (Figure 1A and myeloid gating illustrated in Figure E1). The MerTK$^+$CD64$^+$ macrophages were further examined using CD11c versus CD11b or MHCII to illustrate AMs and IMs. AMs were SiglecF$^+$CD11c$^+$CD11b$^-$ and all IMs were SiglecF$^-$CD11b$^+$ (Figures 1A and E1). The IMs, which represent 9% of all pulmonary myeloid cells, were further distinguished into three populations based on their expression levels of CD11c and MHCII: CD11c^{lo}MHCII^{lo} (which we termed "IM1"); CD11c^{lo}MHCII^{hi} (IM2); and CD11c$^+$MHCII^{hi} (IM3) (Figures 1A–1C). Next, the gate containing MerTK$^-$CD64$^{lo/-}$ cells, macrophage-deficient cells, was examined using CD11c versus MHCII. Dual-positive cells for CD11c and MHCII displayed the two known DC populations: CD103$^+$CD11b^{lo} DCs (Batf3$^+$ DCs) and CD103$^-$CD11b$^+$ DCs (Irf4$^+$ DCs) (13). Furthermore, by size, IMs and DCs exhibited high granularity compared with monocytes, which were much smaller (Figure 1D). The remaining gate MerTK$^-$CD64$^{lo/-}$CD11c$^{int/-}$MHCII$^{int/-}$ cells, macrophage/DC–deficient cells, was plotted as side scatter versus F480 to illustrate monocytes, neutrophils, and eosinophils (Figure 1A) (14), of which most were in the intravascular space (Figure E1). Finally, we confirmed that all seven pulmonary mononuclear phagocytes identified (AMs, three IMs, two DCs, and a few Ly6C$^{+/int}$MHCII$^+$ monocytes) were extravascular and not intravascular by injecting fluorescently conjugated anti-CD45 into the circulation to label and exclude intravascular leukocytes from our analysis (Figure E1) (15, 16).

Next, RNA sequencing was performed to assess the transcriptional signatures expressed by pulmonary IMs compared with AMs (IM sorting strategy Principal component analysis demonstrated that IMs were clearly. Principal component analysis demonstrated that the three IMs were clearly distinct from AMs and from each other (Figure 2A). First, we assessed whether IMs, like AMs, exhibit a macrophage signature (12). Indeed, both IMs and AMs highly expressed *bona fide* macrophage genes, such as *MerTK*, *Fcgr1* (*CD64*), *Emr1* (*F4/80*), *CD68*, *Lysozyme 2*, *Lamp1*, and *CD36*, while lacking hallmark DC genes, such as *CCR7*, *Dpp4* (CD26), and *Zbtb46* (Figure 2B) (17–21). However, there were also some major differences between AMs and IMs. Notably, unique cell surface molecules that are commonly used to identify AMs (22–24) were absent in all three IM groups. These included *Marco*, *Siglec-F*, and *Csf2r* (granulocyte/macrophage colony–stimulating factor receptor) (Figure 2B). In contrast, genes shown to report monocyte/macrophage linage (25) and repress self-renewal (26, 27), such as *Mafb* and *Maf*, were expressed by IMs, but not AMs, which were previously identified as self-renewing (14). Furthermore, IMs are thought to arise from postnatal monocytes (22, 28, 29) and monocyte-related genes, such as *CD14*, *CD163*, and *Csfr1* (macrophage colony-stimulating factor [M-CSF] receptor) were highly expressed on IMs compared with AMs (Figure 2B) (30). These data suggest that IMs may derive from circulating monocytes, but how often is unclear.

Next, we investigated whether the three IMs could be defined by a programing state (i.e., proinflammatory or reparative, classical or alternative, or "M1" versus "M2" like) (31, 32). However, in the naive noninflamed lung, there was no clear distinction between the three IMs for these types of programing markers (Figure 2C). On the other hand, compared with the AMs, all three of the IMs expressed higher levels of inflammatory mediators and receptors, specifically complement components *C1qa*, *C1qb*, and *C1qc* (Figures 2C and E3). In addition, several chemokine ligands, *CCL7*, *CCL8*, and *CCL12*, involved in reparative functions were expressed on IM1 and IM2 compared

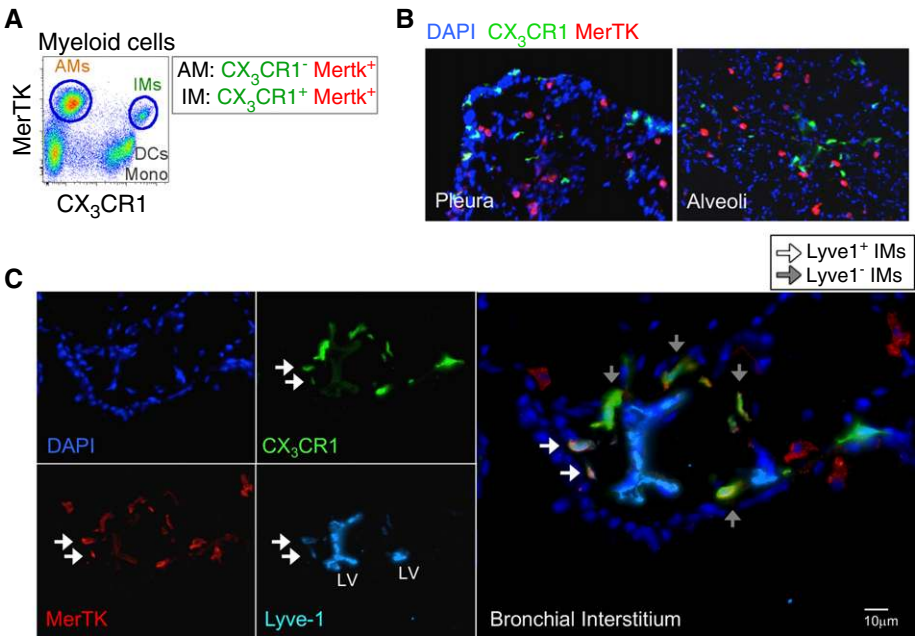

Figure 6. IMs are located in the bronchial interstitium. (*A*) FACS analysis of gated pulmonary myeloid cells from naive CX_3CR1^{GFP} mice plotted as MerTK versus CX_3CR1. (*B* and *C*) Frozen sections from CX_3CR1^{GFP} reporter mice (*green*) were stained with antibody against MerTK (*red*) and 4′,6-diamidino-2-phenylindole (DAPI; *blue*). (*B*) Pleural and alveolar space images (20× magnification) were analyzed for the presence of double-positive CX_3CR1^+ $MerTK^+$ IMs. (*C*) Bronchial interstitium was also stained for Lyve-1 (*cyan*) to identify lymphatic vessels (LV) and Lyve-1^+ IMs (40× magnification). *Arrows* identify CX_3CR1^+ $MerTK^+$ IMs; *white arrows* point to Lyve-1^+ IMs and *gray arrows* point to Lyve-1^- IMs. Images are representative of the indicated regions of lung tissue surveyed over five experiments. *Scale bar*, 10 μm.

with IM3 (33, 34). In summary, gene expression analysis highlighted differences between AMs and IMs, along with a strong macrophage signature in general.

We next investigated the correlation of mRNA with protein expression (28, 35–37). As illustrated in Figure 3, all pulmonary macrophages expressed cell surface molecules F4/80, CD36, CD64, and CD206, although IM1 and IM2 expressed more CD206 than IM3. CD14 was solely expressed by IMs and not AMs (Figure E4). Focusing on differences between the IMs, IM1 and IM2 expressed more Lyve-1 and CD169 compared with IM3. In contrast, IM3 expressed elevated levels of CCR2 and CD11c compared with IM1 and IM2 (Figure 3A). When the IMs were analyzed for the expression of CX_3CR1, Csf1r, and Zbtb46 using reporter mice, all three IMs expressed high levels of CX_3CR1 and Csf1r, and virtually no Zbtb46, a transcription factor expressed by endothelial cells, classical DCs, and their precursors (18, 19) (Figure 3A). Table 1 provides a summary of the gene and protein expression analyzed in the seven pulmonary mononuclear phagocytes identified in Figure 1A. Overall, the genes and proteins examined for pulmonary IMs closely align.

Because the IMs displayed a macrophage signature, one of the most functional characteristic of macrophages in general is their ability to engulf large exogenous beads, cells, and microbes. Therefore, we examined the IMs' phagocytic ability using carboxylated beads or microbial particles (*E. coli* bioparticles, *Staphylococcus aureus* bioparticles, or zymosan A bioparticles). First, uptake of particulates *in vivo* demonstrated that IM1 and IM2 appear to acquire microbial particulates more readily than IM3 (Figure 4). However, when *ex vivo* experiments were performed to eliminate the constraint of the lung architecture and allow for equal access of particulates, there was no clear difference in the uptake of beads by AMs or IMs. On the other hand, zymosan bioparticles appeared to be more actively taken up by IM3 compared with IM1, IM2, and AMs (Figure 4). Overall, *ex vivo* data support a common macrophage function for the three IMs as highly phagocytic.

IMs Display a Slow Turnover Rate

Next, we investigated the proliferation and relative rate of IM turnover. To assess proliferation, wild-type mice were injected daily with BrdU to examine its incorporation into $Ly6C^+$ monocytes (thought to be IM precursor cells) and IMs. By Days 3 and 6, blood $Ly6C^+$ monocytes were highly labeled with BrdU, approximately 78 and 94% (Figure E5). However, by Day 6, the incorporation of BrdU in IMs was approximately 15–30%, similar to AMs, and substantially lower than $Ly6C^+$ monocytes (Figure E5), suggesting that $Ly6C^+$ monocytes are not rapidly, if at all, replenishing IMs in steady state.

To further distinguish the rate of IM turnover, we used two complementary approaches. The first approach was to create BM chimeras to monitor donor-derived replenishment of host AMs and IMs. To create BM chimeric mice, host CD45.1 mice were lethally irradiated with lead strips across their thorax. These strips protect the AMs and IMs from γ radiation, while reconstituting CD45.1 host with donor CD45.2 BM cells (38). At 5 weeks after irradiation, the frequency of donor-derived cells was assessed in IMs. IM3 demonstrated more donor cell replenishment compared with IM1 and IM2, with IM1 having the lowest level of replacement (Figure 5A). These data suggest that IM3 more readily replenishes from circulating precursor cells than IM1 and IM2.

Parabiotic mice were used as an additional means of assessing the rate of IM turnover. In this model, congenic mice were surgically joined together to exchange circulatory blood. The relative rate of IM turnover was measured by the frequency of contribution from the partner mouse. At 15 weeks after surgical joining, IM3, compared with IM2 and IM1, contained more donor-derived cells (Figure 5B), supporting the concept that IM3 indeed replenishes its population from circulating precursor cells more readily than IM1 and IM2. Furthermore, we observed that the partner contribution to all IM subtypes was similar to AMs (analyzed by digestion and not bronchoalveolar lavage), and was significantly lower than that of interstitial pulmonary monocytes (14), suggesting that IMs are long lived, and either slowly self-renewing or sporadically replenished by circulating monocytes. Combined, these

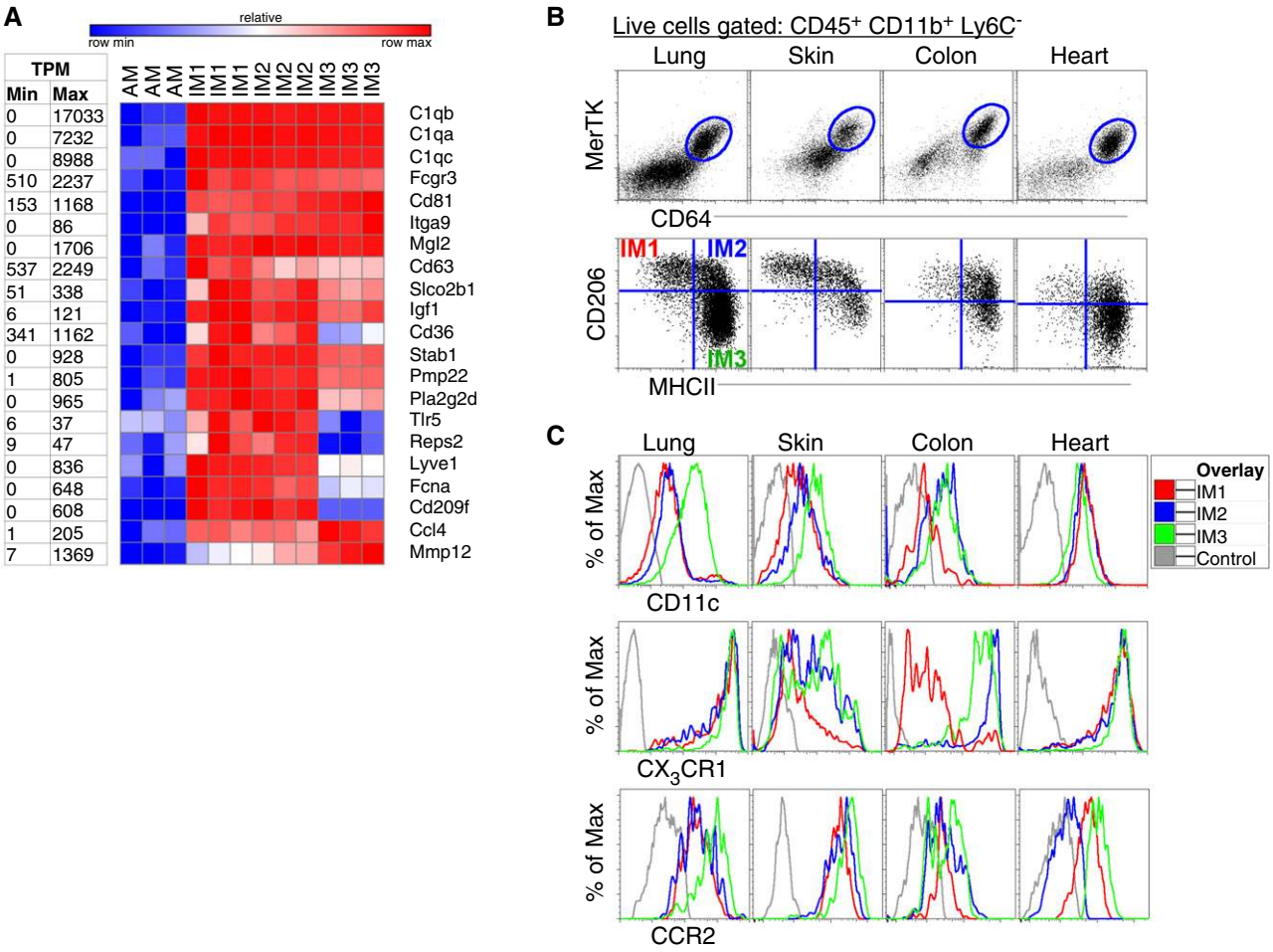

Figure 7. Three IMs are also present in other organs. (*A*) RNA-seq data were analyzed for the expression of genes previously associated with dermal or cardiac IMs. Heat map shows the relative transcript expression by AMs compared with IM1, IM2, and IM3. *Rows* are displayed as signal intensity relative to minimum and maximum, values with minimum and maximum TPM counts displayed to the *left* of each *row*. (*B* and *C*) The presence of IMs was analyzed in naive WT or CX_3CR1^{GFP} mice in the lung, skin, colon, and heart. (*B*) $CD45^+CD11b^+Ly6C^-$ cells were plotted as MerTK versus CD64 to identify $MerTK^+CD64^+$ macrophages (*upper panel*). Gated macrophages were then plotted as CD206 versus MHCII (*lower panel*). Data are representative of four independent experiments with $n = 3$. (*C*) Histograms display overlays of all three IMs for the expression of CD11c, CX_3CR1 (reported), and CCR2 from the indicated organs. *Gray lines* illustrate isotype control antibody or WT (GFP^-) controls.

data demonstrate that the rate of IM turnover differs among the three IMs, with IM3 displaying the highest turnover rate.

IMs Are Located within the Bronchial Interstitium and Not the Alveolar Interstitium

Next, we investigated the location of pulmonary IMs using the $CX_3CR1^{gfp/+}$ reporter mice and immunostaining for MerTK (Figures 6 and E6). The flow plot in Figure 6A illustrates how the expression of CX_3CR1 distinguishes $MertK^+$ IMs (CX_3CR1^+) from AMs (CX_3CR1^-). All other CX_3CR1^+ cells are $MertK^-$ (monocytes, $Irf4^+$ DCs, and natural killer cells). Accordingly, IMs are the only cells that double label with CX_3CR1 and MerTK (Figure 6A) (14). Immunohistochemistry staining with MerTK, to identify macrophages, and Lyve-1, to identify lymphatic vessels, of lung sections demonstrated the presence of dual-positive MerTK (*red*) and CX_3CR1 (*green*) IMs in the bronchial interstitium and bronchovascular bundles, but not in the pleura or alveoli (Figures 6B, 6C, and E6). In contrast, AMs ($MerTK^+CX_3CR1^-$) were clearly observed in the alveolar lumen (Figures 6B and E6), but not within the bronchial tissues. Interestingly, we were able to observe both $Lyve\text{-}1^+$ and $Lyve\text{-}1^-$ IMs close to lymphatic vessels, also located within the bronchial interstitium (Figure 6C). These data demonstrate that, in a naive mouse, all three IMs are located within the bronchial interstitium and not alveolar interstitium.

IMs, Like DC Subtypes, Are Present in Other Organs besides the Lung

Unlike organ-specific macrophages (i.e., AMs, Langerhans cells, microglia, Kupffer cells, red-pulp macrophages, and peritoneal macrophages) that display their own unique transcriptional signature and function (12, 39), IMs appear to have overlapping transcriptional profiles within multiple organs (28, 35–37) (Figures 7A and E3). We hypothesize that, like DCs, IMs maintain their overall transcriptional profile and function regardless of the organ in which they reside. To support this hypothesis, we analyzed the top IM genes

Table 1. Phenotype of Pulmonary Mononuclear Phagocytes

Protein Expression	Pulmonary Cell Type						
	AM	IM1	IM2	IM3	Ly6C$^+$ mo	Batf3$^+$ DC	Irf4$^+$ DC
MerTK	+	+	+	+	−	−	−
CD64	+	+	+	+	lo	−	−
F4/80	+	+	+	+	lo	−	lo
CD11b	−	+	+	+	+	lo	+
CD11c	+	−	−	+	−/int	+	+
MHCII	−	lo	+	+	−/lo/+	+	+
CD206	+	+	+	lo	lo	−	lo/+
CD169	+	+	+	−	−	−	−
CD36	+	+	+	+	+	+	−
Lyve-1	−	+	+/−	−	−	−	−
CX_3CRI	−	++	++	++	+	−	+
Csf1r	+/−	+	+	+	+	lo	+
CCR2	−	−	−/lo	+	+	lo	lo
Zbtb46	−	−	−	−	−	+	+

Definition of abbreviations: AM, alveolar macrophage; Batf3, basic leucine zipper transcriptional factor ATF-like 3; CCR2, C-C motif chemokine receptor 2; Csf1r, colony stimulating factor 1 receptor; CX_3CRI, fractalkine receptor; DC, dendritic cell; IM, interstitial macrophage; int, intermediate; Irf4, interferon regulatory factor 4; lo, low; Ly6C, lymphocyte antigen 6 complex; Ly6C$^+$ mo, Ly6C$^+$ monocytes; Lyve-1, lymphatic vessel endothelial hyaluronan receptor 1; MerTK, MER proto-oncogene, tyrosine kinase; MHCII, major histocompatibility complex class II; Zbtb46, zinc finger and BTB domain containing 46.

previously reported in the skin and heart (referred to in the literature as P4 or R2 for IM1, P5 or R1 for IM2, and P3 or R8 for IM3) (28, 35–37), and observed a similar gene expression profile for all three IMs reported in the lungs (Figure 7A). In addition, we extended our gating strategy using MertK, CD64, and CD11b to identify IMs in skin, heart, and gut. Like the lung, skin, heart, and gut contained three MertK$^+$CD64$^+$ populations of IMs (Figure 7B). However, there were a few differences, such as that heart IMs did not express high levels CD11c and skin IMs expressed moderate to low levels of CX_3CR1 (Figure 7C) (35, 37). Overall, these findings suggest that three IMs, like the two main DC subsets, are present in other organs besides the lung (5, 39–41).

Discussion

In this study, we newly identified and characterized three pulmonary IMs. All three IMs displayed a strong transcriptional macrophage signature, which includes the expression of *MerTK*, *CD64*, *CD68*, *F4/80*, *Mafb*, and *Lamp1*, while lacking the classical DC chemokine receptor and transcription factor, *CCR7* and *Zbtb46*. In addition, all three of the IM populations were large and highly phagocytic, supporting their designation as macrophages.

Principal component analysis of the pulmonary mononuclear phagocytes transcriptomes illustrated that IMs were distinct from AMs and each other. Moreover, both transcriptome and protein analyses demonstrated that the three IMs differentially expressed proinflammatory cytokines, chemokine ligands, MHCII, CD11c, CD206, and Lyve-1, among other genes. Nonetheless, all three IMs expressed high levels of CX_3CR1 and CD14. CX_3CR1 and CD14 are required for the development of Ly6C$^-$ monocytes and monocyte-derived DCs (42, 43). However, we observed that neither CX_3CR1 nor CD14 was required for IM survival (Figure E5 and data not shown). All in all, there were substantial similarities and differences between the IMs at both the transcriptional and protein level, although how these differences influence their functional roles in tissue will require further investigation.

Experiments with BrdU-treated mice, lung-shielded BM chimeras, and parabiotic mice demonstrated that IMs display a relatively slow turnover rate, even lower than that of AMs. Notably, IM3 was more readily replaced by circulating precursor cells than IM1 and IM2. At a glance, IM3 appears to resemble pulmonary monocytes containing high levels of CCR2, TNF-α, and IL-1β expression. However, more investigations are required to support a relationship between IM3 and nonlymphoid monocytes.

IMs are thought to derive from postnatal Ly6C$^+$ monocytes (28, 29). Our data show that BM donor–derived cells significantly replenished IMs at 5 weeks after irradiation with lung shielding. However, the replenishment of IMs by BM donor–derived cells alone does not definitely prove that IMs derive from postnatal CCR2$^+$Ly6C$^+$ monocytes, but instead proves that IMs *can* derive from a postnatal precursor cell that depends on CCR2 for migration into tissue (28). Without linage tracing mice, it still remains unclear whether pulmonary IMs develop during embryogenesis like AMs, or after birth. *Ergo*, in the context of radiation studies, replenishment by BM-donor cells is inevitable. Many questions remain as to how IMs are maintained and function, not only during homeostasis, but also during inflammation. For example, during inflammation, do IMs, like AMs, self-renew, or are they replenished by recruited monocytes or precursor cells? This question will be challenging to address, as recruited monocytes that are present during inflammation acquire many IM features (data not shown).

Finally, other studies have observed three IM populations in the skin, heart, and gut (28, 35–37). The IMs described in these studies appear to share many of the same cell surface molecules and top transcribed genes as observed in the lung, particularly the expression of *CD64*, *F4/80*, *MerTK*, *CD11b*, *CD206*, *CCR2*, *MHCII*, *C1q*, *Lyve-1*, *Mgl2*, and *Stab1*. This led us to investigate whether our gating strategy would identify IMs in other organs. Indeed, we observed three IMs in the gut, skin, and heart with minor differences. Overall, these data lead us to hypothesize that the IM subtypes, like DC subtypes, most likely maintain a similar transcriptional profile and function regardless of the organ in which they reside, which is in striking contrast to tissue-specific macrophages (i.e., AMs, Langerhans cells, microglia, red-pulp macrophages, and peritoneal macrophages), of which the function and differentiation is dictated by the environment in which they reside in (5, 22, 23, 44). ■

Author disclosures are available with the text of this article at www.atsjournals.org.

Acknowledgments: The authors thank Dr. Cory M. Hogaboam for his insight in macrophage biology and Dr. Courtney Frasch for her assistance in isolating gut interstitial macrophages.

References

1. Schneider C, Nobs SP, Kurrer M, Rehrauer H, Thiele C, Kopf M. Induction of the nuclear receptor PPAR-γ by the cytokine GM-CSF is critical for the differentiation of fetal monocytes into alveolar macrophages. *Nat Immunol* 2014;15:1026–1037.
2. Hoeffel G, Chen J, Lavin Y, Low D, Almeida FF, See P, Beaudin AE, Lum J, Low I, Forsberg EC, *et al*. C-Myb^{+} erythro-myeloid progenitor-derived fetal monocytes give rise to adult tissue-resident macrophages. *Immunity* 2015;42:665–678.
3. Sheng J, Ruedl C, Karjalainen K. Most tissue-resident macrophages except microglia are derived from fetal hematopoietic stem cells. *Immunity* 2015;43:382–393.
4. Bedoret D, Wallemacq H, Marichal T, Desmet C, Quesada Calvo F, Henry E, Closset R, Dewals B, Thielen C, Gustin P, *et al*. Lung interstitial macrophages alter dendritic cell functions to prevent airway allergy in mice. *J Clin Invest* 2009;119:3723–3738.
5. Scott CL, Henri S, Guilliams M. Mononuclear phagocytes of the intestine, the skin, and the lung. *Immunol Rev* 2014;262:9–24.
6. Janssen, W. J. *et al*. Fas determines differential fates of resident and recruited macrophages during resolution of acute lung injury. *Am J Respir Crit Care Med* 2011;184:547–560.
7. Kamran P, Sereti KI, Zhao P, Ali SR, Weissman IL, Ardehali R. Parabiosis in mice: a detailed protocol. *J Vis Exp* 2013;(80): doi: 10.3791/50556.
8. Liao Y, Smyth GK, Shi W. featureCounts: an efficient general purpose program for assigning sequence reads to genomic features. *Bioinformatics* 2014;30:923–930.
9. Love MI, Huber W, Anders S. Moderated estimation of fold change and dispersion for RNA-seq data with DESeq2. *Genome Biol* 2014;15: 550.
10. Team RCR. A language and environment for statistical computing. Vienna: R Foundation for Statistical Computing. 2014 [accessed 2017 May 22]. Available from: http://www.r-project.org
11. Kanehisa M, Goto S, Sato Y, Kawashima M, Furumichi M, Tanabe M. Data, information, knowledge and principle: back to metabolism in KEGG. *Nucleic Acids Res* 2014;42:D199–D205.
12. Gautier EL, Shay T, Miller J, Greter M, Jakubzick C, Ivanov S, Helft J, Chow A, Elpek KG, Gordonov S, *et al*.; Immunological Genome Consortium. Gene-expression profiles and transcriptional regulatory pathways that underlie the identity and diversity of mouse tissue macrophages. *Nat Immunol* 2012;13:1118–1128.
13. Desch AN, Gibbings SL, Clambey ET, Janssen WJ, Slansky JE, Kedl RM, Henson PM, Jakubzick C. Dendritic cell subsets require *cis*-activation for cytotoxic CD8 T-cell induction. *Nat Commun* 2014;5: 4674.
14. Jakubzick C, Gautier EL, Gibbings SL, Sojka DK, Schlitzer A, Johnson TE, Ivanov S, Duan Q, Bala S, Condon T, *et al*. Minimal differentiation of classical monocytes as they survey steady-state tissues and transport antigen to lymph nodes. *Immunity* 2013;39:599–610.
15. Anderson KG, Mayer-Barber K, Sung H, Beura L, James BR, Taylor JJ, Qunaj L, Griffith TS, Vezys V, Barber DL, *et al*. Intravascular staining for discrimination of vascular and tissue leukocytes. *Nat Protoc* 2014;9:209–222.
16. Desch AN, *et al*. Flow cytometric analysis of mononuclear phagocytes in non-diseased human lung and lung-draining lymph nodes. *Am J Respir Crit Care Med* 2016;193:614–626.
17. Gautier EL, Chow A, Spanbroek R, Marcelin G, Greter M, Jakubzick C, Bogunovic M, Leboeuf M, van Rooijen N, Habenicht AJ, *et al*. Systemic analysis of PPARγ in mouse macrophage populations reveals marked diversity in expression with critical roles in resolution of inflammation and airway immunity. *J Immunol* 2012;189: 2614–2624.
18. Satpathy AT, Kc W, Albring JC, Edelson BT, Kretzer NM, Bhattacharya D, Murphy TL, Murphy KM. Zbtb46 expression distinguishes classical dendritic cells and their committed progenitors from other immune lineages. *J Exp Med* 2012;209:1135–1152.
19. Meredith MM, Liu K, Darrasse-Jeze G, Kamphorst AO, Schreiber HA, Guermonprez P, Idoyaga J, Cheong C, Yao KH, Niec RE, *et al*. Expression of the zinc finger transcription factor zDC (Zbtb46, Btbd4) defines the classical dendritic cell lineage. *J Exp Med* 2012;209: 1153–1165.
20. Contreras V, Urien C, Guiton R, Alexandre Y, Vu Manh TP, Andrieu T, Crozat K, Jouneau L, Bertho N, Epardaud M, *et al*. Existence of CD8alpha-like dendritic cells with a conserved functional specialization and a common molecular signature in distant mammalian species. *J Immunol*2010;185:3313–3325.
21. Förster R, Schubel A, Breitfeld D, Kremmer E, Renner-Müller I, Wolf E, Lipp M. CCR7 coordinates the primary immune response by establishing functional microenvironments in secondary lymphoid organs. *Cell* 1999;99:23–33.
22. Gibbings SL, Goyal R, Desch AN, Leach SM, Prabagar M, Atif SM, Bratton DL, Janssen W, Jakubzick CV. Transcriptome analysis highlights the conserved difference between embryonic and postnatal-derived alveolar macrophages. *Blood* 2015;126: 1357–1366.
23. Lavin Y, Winter D, Blecher-Gonen R, David E, Keren-Shaul H, Merad M, Jung S, Amit I. Tissue-resident macrophage enhancer landscapes are shaped by the local microenvironment. *Cell* 2014;159: 1312–1326.
24. Guilliams M, De Kleer I, Henri S, Post S, Vanhoutte L, De Prijck S, Deswarte K, Malissen B, Hammad H, Lambrecht BN. Alveolar macrophages develop from fetal monocytes that differentiate into long-lived cells in the first week of life via GM-CSF. *J Exp Med* 2013; 210:1977–1992.
25. Wu X, Briseño CG, Durai V, Albring JC, Haldar M, Bagadia P, Kim KW, Randolph GJ, Murphy TL, Murphy KM. Mafb lineage tracing to distinguish macrophages from other immune lineages reveals dual identity of Langerhans cells. *J Exp Med* 2016;213: 2553–2565.
26. Aziz A, Soucie E, Sarrazin S, Sieweke MH. MafB/c-Maf deficiency enables self-renewal of differentiated functional macrophages. *Science* 2009;326:867–871.
27. Soucie EL, Weng Z, Geirsdóttir L, Molawi K, Maurizio J, Fenouil R, Mossadegh-Keller N, Gimenez G, VanHille L, Beniazza M, *et al*. Lineage-specific enhancers activate self-renewal genes in macrophages and embryonic stem cells. *Science* 2016;351: aad5510.
28. Plantinga M, Guilliams M, Vanheerswynghels M, Deswarte K, Branco-Madeira F, Toussaint W, Vanhoutte L, Neyt K, Killeen N, Malissen B, *et al*. Conventional and monocyte-derived CD11b(+) dendritic cells initiate and maintain T helper 2 cell–mediated immunity to house dust mite allergen. *Immunity* 2013;38:322–335.
29. Bain CC, Bravo-Blas A, Scott CL, Gomez Perdiguero E, Geissmann F, Henri S, Malissen B, Osborne LC, Artis D, Mowat AM. Constant replenishment from circulating monocytes maintains the macrophage pool in the intestine of adult mice. *Nat Immunol* 2014; 15:929–937.
30. Larson SR, Atif SM, Gibbings SL, Thomas SM, Prabagar MG, Danhorn T, Leach SM, Henson PM, Jakubzick CV. Ly6C(+) monocyte efferocytosis and cross-presentation of cell-associated antigens. *Cell Death Differ* 2016;23:997–1003.
31. Mills CD, Harris RA, Ley K. Macrophage polarization: decisions that affect health. *J Clin Cell Immunol* 2015;6:364.
32. Murray PJ, Allen JE, Biswas SK, Fisher EA, Gilroy DW, Goerdt S, Gordon S, Hamilton JA, Ivashkiv LB, Lawrence T, *et al*. Macrophage activation and polarization: nomenclature and experimental guidelines. *Immunity* 2014;41:14–20.
33. Choi ES, Jakubzick C, Carpenter KJ, Kunkel SL, Evanoff H, Martinez FJ, Flaherty KR, Toews GB, Colby TV, Kazerooni EA, *et al*. Enhanced monocyte chemoattractant protein-3/CC chemokine ligand-7 in usual interstitial pneumonia. *Am J Respir Crit Care Med* 2004;170: 508–515.
34. Moore BB, Murray L, Das A, Wilke CA, Herrygers AB, Toews GB. The role of CCL12 in the recruitment of fibrocytes and lung fibrosis. *Am J Respir Cell Mol Biol* 2006;35:175–181.
35. Tamoutounour S, Guilliams M, Montanana Sanchis F, Liu H, Terhorst D, Malosse C, Pollet E, Ardouin L, Luche H, Sanchez C, *et al*. Origins and functional specialization of macrophages and of conventional and monocyte-derived dendritic cells in mouse skin. *Immunity* 2013; 39:925–938.
36. Tamoutounour S, Henri S, Lelouard H, de Bovis B, de Haar C, van der Woude CJ, Woltman AM, Reyal Y, Bonnet D, Sichien D, *et al*. CD64 distinguishes macrophages from dendritic cells in the gut and

reveals the Th1-inducing role of mesenteric lymph node macrophages during colitis. *Eur J Immunol* 2012;42:3150–3166.
37. Epelman S, Lavine KJ, Beaudin AE, Sojka DK, Carrero JA, Calderon B, Brija T, Gautier EL, Ivanov S, Satpathy AT, *et al*. Embryonic and adult-derived resident cardiac macrophages are maintained through distinct mechanisms at steady state and during inflammation. *Immunity* 2014;40:91–104.
38. Janssen WJ, Muldrow A, Kearns MT, Barthel L, Henson PM. Development and characterization of a lung-protective method of bone marrow transplantation in the mouse. *J Immunol Methods* 2010;357:1–9.
39. Okabe Y, Medzhitov R. Tissue biology perspective on macrophages. *Nat Immunol* 2016;17:9–17.
40. Guilliams M, Ginhoux F, Jakubzick C, Naik SH, Onai N, Schraml BU, Segura E, Tussiwand R, Yona S. Dendritic cells, monocytes and macrophages: a unified nomenclature based on ontogeny. *Nat Rev Immunol* 2014;14:571–578.
41. Ginhoux F, Liu K, Helft J, Bogunovic M, Greter M, Hashimoto D, Price J, Yin N, Bromberg J, Lira SA, *et al*. The origin and development of nonlymphoid tissue CD103+ DCs. *J Exp Med* 2009;206: 3115–3130.
42. Cheong C, Matos I, Choi JH, Dandamudi DB, Shrestha E, Longhi MP, Jeffrey KL, Anthony RM, Kluger C, Nchinda G, *et al*. Microbial stimulation fully differentiates monocytes to DC-SIGN/CD209(+) dendritic cells for immune T cell areas. *Cell* 2010;143:416–429.
43. Landsman L, Bar-On L, Zernecke A, Kim KW, Krauthgamer R, Shagdarsuren E, Lira SA, Weissman IL, Weber C, Jung S. CX3CR1 is required for monocyte homeostasis and atherogenesis by promoting cell survival. *Blood* 2009;113:963–972.
44. van de Laar L, Saelens W, De Prijck S, Martens L, Scott CL, Van Isterdael G, Hoffmann E, Beyaert R, Saeys Y, Lambrecht BN, *et al*. Yolk sac macrophages, fetal liver, and adult monocytes can colonize an empty niche and develop into functional tissue-resident macrophages. *Immunity* 2016;44:755–768.